Joint 48th IEEE Conference on Decision and Control and
28th Chinese Control Conference
Shanghai, P.R. China, December 16-18, 2009

Feasibility of a Distributed Flight Array

Raymond Oung, Alireza Ramezani, Raffaello D'Andrea

Abstract— **This paper introduces the Distributed Flight Array (DFA) which is being developed at ETH Zurich. This multi-rotor platform consists of autonomous rotor modules that are able to drive, dock with their peers, and fly in a coordinated fashion. These modules are organized as distributed computational units with minimal sensory input. This is a complex system that is rich in dynamics with much room to explore various strategies of distributed estimation and control. In this paper, a simple distributed strategy for hover control is presented and feasibility of the DFA is demonstrated.**

I. Introduction

Vertical take-off and landing vehicles (VTOL) have gained popularity within the aerial vehicles community over the last few years. A particular advantage they have over most aerial vehicles is their unique ability for vertical stationary flight. Moreover, they provide an excellent platform for exploiting advanced sensor technology, pushing the limits of energy storage, and investigating techniques in automatic control.

Until now, researchers in this area have focussed primarily on quadrotor platforms [1], [2], [3], [4]. The Institute for Dynamic Systems and Control at ETH Zurich has extended this design to a multi-rotor platform with distributed control, which has been designated the Distributed Flight Array (DFA). The DFA consists of individual modules that are able to drive autonomously and assemble with their peers on the ground. Each module can generate enough thrust using a single fixed propeller to lift itself into the air, but is unstable in flight. Not until they are joined do these relatively simple modules evolve into a sophisticated multi-propeller system capable of coordinated flight, see Fig. 1. The goal is to have many modules assemble at random, fly to a predetermined altitude, hover, break apart, fall back down, and repeat the cycle. This abstract testbed features rich dynamics and challenging design problems, and will undoubtedly be an eye-catching pedagogical showpiece for distributed estimation and control.

Fig. 1. Shown in this figure is a concept representation of the DFA in a random configuration. The array is composed of interconnected rotor modules that communicate with one another for coordinated flight.

The authors are with the Institute for Dynamic Systems and Control, ETH Zurich, Switzerland. R. Oung is the corresponding author (roung@ethz.ch).

This project comprises three key areas of interest: 1) Each DFA module must be optimized for weight, strength, and durability. The design challenges mirror those of modular reconfigurable robots [5] and micro aerial vehicles [3], which include electromechanical interconnection, inter-module communication, and energy storage. 2) Modules must be able to drive and dock reliably with peers using a minimum number of sensors in order to reduce design complexity and energy usage. 3) The DFA must be able to fly in a coordinated fashion regardless of the array's configuration. A distributed estimation and control strategy will be developed for flight; distributed systems can be made scalable and robust to module failure [6].

This paper focuses on the third key area of interest, distributed flight control. The outline of this paper is as follows. In Section II, a brief system description of a DFA module is given. Section III presents a linearized dynamic model of the DFA and demonstrates that the force/torque response characteristics of a module around the hovering thrust are well approximated as first-order. This model is used in Section IV, where a simple distributed strategy for hover control is derived, followed by simulation results that prove feasibility of the DFA for a small and large set of modules. Simulation results for a four module array are shown to be consistent with experimental results in Section V. Concluding remarks are made in Section VI.

II. Module Description

Each DFA module resembles a hexagon with 3D extrusions designed for passive alignment and docking, see Fig. 2. The chassis is composed of a low-density ethyl polypropylene (EPP) foam. On each side of the chassis is a symmetric arrangement of four permanent magnets that assist in passive alignment during the docking phase and help to keep the modules interconnected during flight. To dock, modules drive on the ground and into each other using a set of three custom made omni-wheels; each wheel is driven by a brushed DC motor with a built-in encoder.

Mounted to the center of the chassis is a brushless DC motor with an off-the-shelf motor controller and a 3-blade propeller capable of producing more than 3 N of thrust. All modules are exactly the same except for propeller orientation, where there are two possible orientations: clockwise (CW) and counterclockwise (CCW). This is necessary in order to cancel aerodynamic torques in trimmed flight.

Custom-designed electronics were made to meet all the on-board sensing, communication, and computation requirements. Each module comes equipped with a 3-axis rate gyro

978-1-4244-3872-3/09/$25.00 ©2009 IEEE

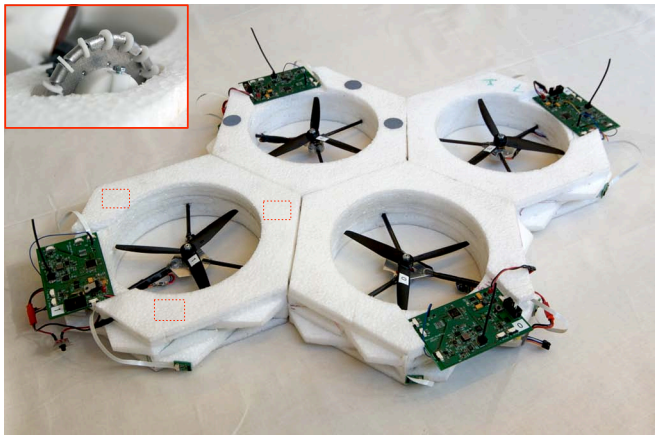

Fig. 2. Shown here are four prototype DFA modules in a docked configuration. The module's chassis resembles a hexagon with 3D extrusions designed for passive alignment and docking; it is made from cut-out sheets of low-density ethyl polypropylene (EPP) foam. The dotted boxes provide a preview of the custom-made omni-wheels which are embedded in the foam and are used to drive the module.

for measuring angular rates and a pressure sensor for measuring altitude. Bi-directional inter-module communication is accomplished with IrDA via a UART peripheral; there is an IrDA transceiver mounted to each side of the module. An ARM7 core microcontroller handles all the required computation needed for estimation and control.

Also embedded in the chassis is a Lithium-Ion Polymer battery that is capable of powering both the motors and electronics for up to 5 minutes of flight. Table I list some of the physical attributes that characterize a DFA module.

TABLE I

PHYSICAL ATTRIBUTES OF A DFA MODULE

Symbol	Description	Value
ℓ	Characteristic length †	0.250 m
-	Propeller duct diameter	0.180 m
m	Mass per module	0.180 kg

† Defined as the distance between opposite faces of a module

III. MODELING

The full dynamics of the DFA can be quite complex if effects like the flexibility of the propellers, aerodynamic effects of the propeller duct, and the forces that keep the modules together are considered. Since the goal is to determine the feasibility of flight for the DFA, the system is simply modeled as a rigid body without any compliant inter-module connections, incorporating a force and torque generation process at each module around the hovering equilibrium.

A. Flight Dynamics

The DFA's body coordinate frame B is defined as the set of orthogonal axes that coincide with the array's center of mass and that is oriented to the principal axes of rotation. A sequence of three rotations described by Euler angles α, β, γ acting along the z-, y-, x-axis in this order describe the orientation of the DFA's body coordinate frame with respect to the inertial coordinate frame.

Let $(\mathrm{x}_i, \mathrm{y}_i)$ be the coordinate location of the module i with respect to the body coordinate frame. The altitude and attitude of the DFA can be controlled by varying the force (or thrust) f_i and torque τ_i produced by each module, see Fig. 3. How these control forces are generated will be described later. The total thrust generated by N modules is the sum of all thrusts produced by each module, $F = \sum_{i=1}^{N} f_i$. The rolling torque is the sum of all thrusts acting along the moment arm y_i, $T_\gamma = \sum_{i=1}^{N} \mathrm{y}_i f_i$. Similarly, the pitching torque is the sum of all thrusts acting along the moment arm x_i, $T_\beta = -\sum_{i=1}^{N} \mathrm{x}_i f_i$. The yawing torque is the sum of all reaction torques produced by each module; it will be shown that the torque can be accurately modeled as a linear function of thrust. Hence, the yawing torque can be expressed as $T_\alpha = \sum_{i=1}^{N} c_i f_i$.

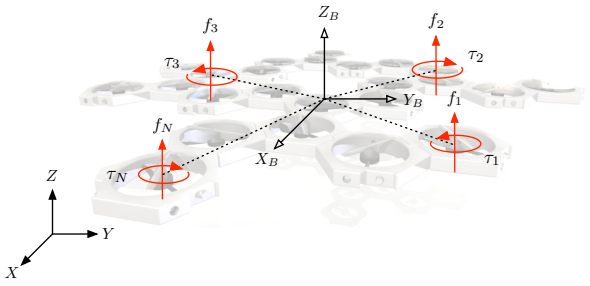

Fig. 3. Shown in this diagram is the inertial coordinate frame and the DFA's body coordinate frame B with force/torque vectors produced by various modules. The body coordinate frame is chosen to coincide with the array's center of mass and is oriented to the principal axes of rotation.

Transforming the total thrust vector F to the inertial coordinate frame results in a translational force along each axis. The translational accelerations $\ddot{x}$ and $\ddot{y}$ in the inertial coordinate frame is a consequence of a pitch β and roll γ rotation, respectively. Since the system is being modeled around the equilibrium, small angles are used to approximate the rotation in γ and β. The rotation in yaw, however, is not assumed to be small. The following set of equations summarize the dynamics of the array to first-order, except for the yaw angle α:

$$Nm\ddot{x} = (\beta \cos\alpha + \gamma \sin\alpha) \sum_{i=1}^{N} f_i \tag{1}$$

$$Nm\ddot{y} = (\beta \sin\alpha - \gamma \cos\alpha) \sum_{i=1}^{N} f_i \tag{2}$$

$$Nm\ddot{z} = \sum_{i=1}^{N} f_i - Nmg \tag{3}$$

$$I_x\ddot{\gamma} = \sum_{i=1}^{N} \mathrm{y}_i f_i \tag{4}$$

$$I_y\ddot{\beta} = -\sum_{i=1}^{N} \mathrm{x}_i f_i \tag{5}$$

$$I_z\ddot{\alpha} = \sum_{i=1}^{N} c_i f_i \tag{6}$$

where Nm is the total mass of the array, (I_x, I_y, I_z) are the principal mass moments of inertia, and g is the acceleration constant due to gravity. Both x and y components of force are written here for the sake of completeness. However, they are not required for hovering and are left out in what follows.

The principal mass moments of inertia can be written as the following:

$$I_x = \epsilon_x \frac{Nm}{4}\left(\frac{\ell\sqrt{N}}{2}\right)^2$$
$$I_y = \epsilon_y \frac{Nm}{4}\left(\frac{\ell\sqrt{N}}{2}\right)^2$$
$$I_z = \epsilon_z \frac{Nm}{2}\left(\frac{\ell\sqrt{N}}{2}\right)^2$$

where $(\epsilon_x, \epsilon_y, \epsilon_z)$ captures the mass distribution of the array.

Assuming that the array configuration is relatively circular, $\frac{\ell\sqrt{N}}{2}$ is comparable to the radius of the array. If this configuration is also full, like a disk, $(\epsilon_x, \epsilon_y, \epsilon_z)$ are expected to be close to 1. In reality, the configuration of the array may be sparse due to unpredictable docking constraints. In such a case, the values of $(\epsilon_x, \epsilon_y, \epsilon_z)$ are expected to be greater than 1.

The equations of motion are normalized in order to gain some intuition on how the size of the array affects flight dynamics:

$$\hat{\mathrm{x}}_i = \frac{\mathrm{x}_i}{\frac{\ell\sqrt{N}}{2}}, \quad \hat{\mathrm{y}}_i = \frac{\mathrm{y}_i}{\frac{\ell\sqrt{N}}{2}}, \quad \hat{c}_i = \frac{c_i}{\ell}, \quad A_i = \frac{f_i}{m}$$

where $\hat{\mathrm{x}}_i$ and $\hat{\mathrm{y}}_i$ are normalized position coordinates and are at most on the order of 1 for a circular array, $\hat{c}_i$ is the normalized force to torque conversion constant and is expected to be much less than 1, and A_i is the normalized thrust in units of acceleration.

The normalized thrust A_i can be broken down into its components, $A_i = \bar{A}_i + a_i$, where $\bar{A}_i$ is the normalized thrust required to establish equilibrium about hover and a_i is the normalized control input. In the special case where there is an equal number of CW and CCW rotating propellers in the array, one can set $\bar{A}_i = g$. In general, however, the system may be over-actuated with an unequal number of CW and CCW rotating propellers. In this case, one can choose the values of $\bar{A}_i$ via least squares, or any other suitable method.

The following set of equations summarize the normalized and linearized equations of motion about hover:

$$\ddot{z} = \frac{1}{N}\sum_{i=1}^{N} a_i \tag{7}$$

$$\hat{I}_x \ddot{\gamma} = \frac{1}{N}\sum_{i=1}^{N} \hat{\mathrm{y}}_i a_i \tag{8}$$

$$\hat{I}_y \ddot{\beta} = -\frac{1}{N}\sum_{i=1}^{N} \hat{\mathrm{x}}_i a_i \tag{9}$$

$$\hat{I}_z \ddot{\alpha} = \frac{1}{N}\sum_{i=1}^{N} \hat{c}_i a_i \tag{10}$$

where

$$\hat{I}_x = \frac{\epsilon_x \ell\sqrt{N}}{8}, \quad \hat{I}_y = \frac{\epsilon_y \ell\sqrt{N}}{8}, \quad \hat{I}_z = \frac{\epsilon_z \ell N}{8} \tag{11}$$

It can be seen from the equations above that the maximum vertical acceleration $\ddot{z}$ is independent of N. The maximum accelerations in roll $\ddot{\gamma}$ and in pitch $\ddot{\beta}$, however, decrease by a factor of $\sqrt{N}$, while the maximum acceleration in yaw $\ddot{\alpha}$ decreases by a factor of N.

Note that the DFA requires at least four modules for hover control; four is the minimum number of control inputs a_i needed to control the four degrees of freedom, Eq. 7 – 10. However, this is only a necessary condition and not a sufficient condition for hover control. For example, four modules lined together in a row would not be linearly stable in attitude. This would lead to a system that is either controllable in roll but not pitch, or vice versa.

B. Force & Torque Generation

The module's force-torque generation unit – motor controller, brushless DC motor, battery, propeller, and propeller duct – is treated as a grey box model consisting of a physical model with some unknown parameters. The input to this system is a pulse-width modulation (PWM) duty cycle D, which effectively controls the angular velocity of the rotor. The output to this system is both the generated force and torque of the module. Voltage of the battery can also be considered as an input to the system. However, the effects of voltage on the dynamics of the system are ignored since the nominal voltage of Lithium-Ion Polymer batteries is relatively constant over the battery cycle. The force-torque characteristics that are described here assume the nominal voltage case around the equilibrium thrust.

Assuming that the force experienced by a module is dominated by the thrust of the rotor, experiments were conducted to verify that force and torque are proportional to the square of the rotor's angular velocity [7]. Measurements of force and torque were made at various duty cycles around the equilibrium thrust. Experimental results show that force and duty cycle can be approximated by an affine relationship, while the torque resulting from the propeller's drag can be approximated as a linear function of thrust, see Fig. 4(a) – 4(b). Other experiments demonstrated the rate of change in angular momentum of the propeller to be negligible. Recall

that this force-torque relationship was used in Eq. 6 and is expressed in the following:

$$\tau_i = cf_i \tag{12}$$

where $c = \pm 1.13 \times 10^{-2}$ m. Note that the sign of c depends on the rotation of the propeller: the sign is positive when the propeller rotates CCW and negative when the propeller rotates CW.

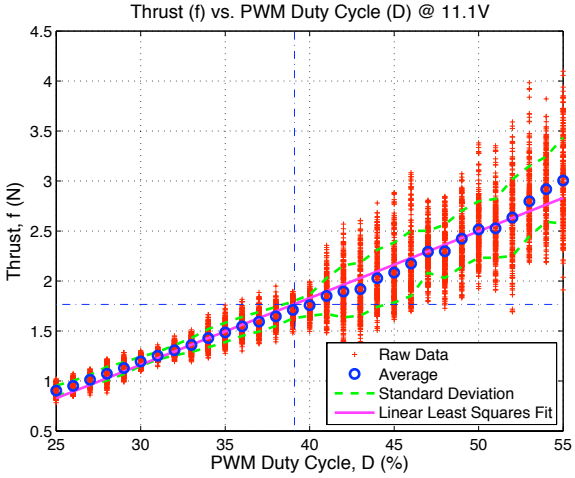

(a) A linear least squares fit of the data relating thrust f to PWM duty cycle D results in the function $f(D) = 6.68 \times 10^{-2}\ D - 8.41 \times 10^{-1}$.

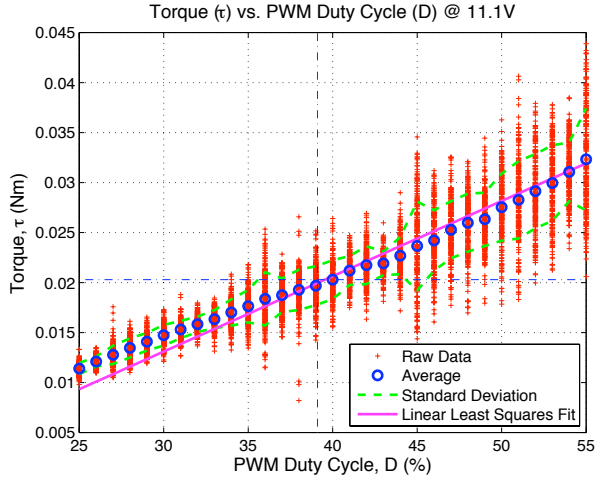

(b) A linear least squares fit to the function $cf(D)$ of the data relating torque τ to PWM duty cycle D results in the function $\tau(D) = 1.13 \times 10^{-2}\ f(D)$.

Fig. 4. Force and torque values were measured with a 6-axis force-torque strain gauge load cell at various PWM duty cycles near equilibrium (approx. D = 39%). At each duty cycle, 500 measurements were made over a period of 5 seconds. The dash-dotted lines in the plots represent the PWM duty cycle that generates equilibrium thrust and the corresponding torque.

Motivated by the results in Fig. 4, the transfer function G_f which relates the input desired thrust $f(D)$ to the output thrust is modeled as a linear time-invariant system. The transfer function that was obtained from the Bode plot of the thrust response, shown in Fig. 5, was found to approximate a first-order system:

$$G_f(s) = \frac{\omega}{s + \omega}$$

where $\omega = 14.3$ rad/s.

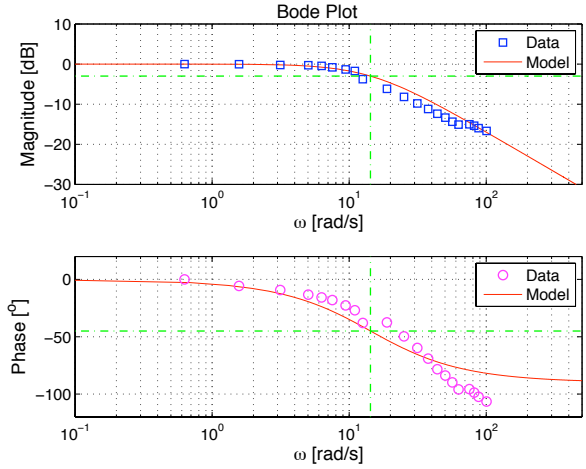

Fig. 5. Bode plot of the thrust response is shown here to approximate a first-order system. Sinusoidal varying duty cycle with an offset equal to the equilibrium thrust and an amplitude equivalent to 0.5 N was sent to the system. Force and torque measurements were made using a 6-axis force-torque strain gauge load cell. The dash-dotted lines in the plots represent the -3 dB frequency, which is 14.3 rad/s, and the corresponding magnitude and phase at this frequency. Note that at high frequencies the measured phase diverges from the model; this is due to unmodeled dynamics, such as delays.

IV. Control

This section presents a simple distributed strategy for hover control based on physical parameters of the DFA. The derivation of this control strategy is generalized, and assumes full state feedback of the system, see Eq. 13. It is assumed that an estimator is used to obtain the state of the system.

Starting with the dynamic model of the DFA that was developed in the previous section, the normalized and linearized equations of motion about the equilibrium, Eq. 7 – 10, can be written as

$$\mathbf{M}\ddot{\mathbf{s}} = \mathbf{P}^T\mathbf{a}$$

where

$$\begin{aligned} \mathbf{M} &= \text{diag}(1, \hat{I}_x, \hat{I}_y, \hat{I}_z) \\ \mathbf{s} &= [z, \gamma, \beta, \alpha]^T \\ \mathbf{a} &= [a_1, \ldots, a_N]^T \end{aligned}$$

The matrix $\mathbf{P}$ contains information pertaining to the configuration of the array and can be written as

$$\mathbf{P} = [\mathbf{p}_z, \mathbf{p}_\gamma, \mathbf{p}_\beta, \mathbf{p}_\alpha]$$

where

$$\mathbf{p}_z = \frac{1}{N}[1, \ldots, 1]^T \qquad \mathbf{p}_\gamma = \frac{1}{N}[\hat{y}_1, \ldots, \hat{y}_N]^T$$
$$\mathbf{p}_\beta = -\frac{1}{N}[\hat{x}_1, \ldots, \hat{x}_N]^T \qquad \mathbf{p}_\alpha = \frac{1}{N}[\hat{c}_1, \ldots, \hat{c}_N]^T$$

The goal is to develop a control strategy that decouples the degrees of freedom. Consider the control strategy of the following form:

$$\mathbf{a} = \mathbf{Q} f(z, \dot{z}, \gamma, \dot{\gamma}, \beta, \dot{\beta}, \alpha, \dot{\alpha}) \tag{13}$$

where

$$\begin{aligned} \mathbf{Q} &= [\mathbf{q}_z, \mathbf{q}_\gamma, \mathbf{q}_\beta, \mathbf{q}_\alpha], \\ f &= [f_z(z, \dot{z}), f_\gamma(\gamma, \dot{\gamma}), f_\beta(\beta, \dot{\beta}), f_\alpha(\alpha, \dot{\alpha})]^T \end{aligned}$$

where the $f.(\cdot)$ are arbitrary functions, to be determined.

The objective is to first design $\mathbf{Q}$ such that $\mathbf{P}^T\mathbf{Q} = \mathbf{I}_4$. This results in the following diagonal system:

$$\begin{aligned} \ddot{z} &= f_z(z, \dot{z}) \\ \hat{I}_x \ddot{\gamma} &= f_\gamma(\gamma, \dot{\gamma}) \\ \hat{I}_y \ddot{\beta} &= f_\beta(\beta, \dot{\beta}) \\ \hat{I}_z \ddot{\alpha} &= f_\alpha(\alpha, \dot{\alpha}) \end{aligned}$$

Note that since $\mathbf{P} \in \mathbb{R}^{N\times 4}$ and $\mathbf{Q} \in \mathbb{R}^{N\times 4}$, the objective is over-determined for an array with more than four modules.

Also note that $\mathbf{p}_z$, $\mathbf{p}_\gamma$, and $\mathbf{p}_\beta$ are orthogonal; this is a result of the chosen coordinate system, see Fig. 3. Moreover, if there are an equal number of CW and CCW modules, then $\mathbf{p}_z$ and $\mathbf{p}_\alpha$ are also orthogonal. In what follows, consider an equal number of CW and CCW modules; the results can readily be generalized.

Let $\mathbf{Q} = \mathbf{P}\mathbf{D}\overline{\mathbf{Q}}$, where

$$\mathbf{D} = \text{diag}\left(\frac{1}{\|\mathbf{p}_z\|^2}, \frac{1}{\|\mathbf{p}_\gamma\|^2}, \frac{1}{\|\mathbf{p}_\beta\|^2}, \frac{1}{\|\mathbf{p}_\alpha\|^2}\right)$$

where $\|\cdot\|$ is the Euclidean norm.

Multiplying $\mathbf{P}^T$ on both sides yields:

$$\begin{aligned} \mathbf{I}_4 &= \mathbf{P}^T\mathbf{Q} = \mathbf{P}^T\mathbf{P}\mathbf{D}\overline{\mathbf{Q}} \\ &= \begin{bmatrix} \|\mathbf{p}_z\|^2 & 0 & 0 & 0 \\ 0 & \|\mathbf{p}_\gamma\|^2 & 0 & \mathbf{p}_\gamma^T\mathbf{p}_\alpha \\ 0 & 0 & \|\mathbf{p}_\beta\|^2 & \mathbf{p}_\beta^T\mathbf{p}_\alpha \\ 0 & \mathbf{p}_\alpha^T\mathbf{p}_\gamma & \mathbf{p}_\alpha^T\mathbf{p}_\beta & \|\mathbf{p}_\alpha\|^2 \end{bmatrix} \mathbf{D}\overline{\mathbf{Q}} \\ &= \begin{bmatrix} 1 & 0 & 0 & 0 \\ 0 & 1 & 0 & e_1 \\ 0 & 0 & 1 & e_2 \\ 0 & e_3 & e_4 & 1 \end{bmatrix} \overline{\mathbf{Q}} \end{aligned}$$

where

$$\begin{aligned} e_1 &= \frac{\mathbf{p}_\gamma^T\mathbf{p}_\alpha}{\|\mathbf{p}_\alpha\|^2} & e_2 &= \frac{\mathbf{p}_\beta^T\mathbf{p}_\alpha}{\|\mathbf{p}_\alpha\|^2} \\ e_3 &= \frac{\mathbf{p}_\alpha^T\mathbf{p}_\gamma}{\|\mathbf{p}_\gamma\|^2} & e_4 &= \frac{\mathbf{p}_\alpha^T\mathbf{p}_\beta}{\|\mathbf{p}_\beta\|^2} \end{aligned}$$

It can readily be shown that,

$$\overline{\mathbf{Q}} = \begin{bmatrix} 1 & 0 \\ 0 & \overline{\overline{\mathbf{Q}}} \end{bmatrix}$$

where

$$\overline{\overline{\mathbf{Q}}} = \frac{1}{1-(e_2e_4+e_3e_1)} \begin{bmatrix} 1-e_2e_4 & e_1e_4 & -e_1 \\ e_2e_3 & 1-e_3e_1 & -e_2 \\ -e_3 & -e_4 & 1 \end{bmatrix}$$

In the special case where there is a large number of CW and CCW modules that are uniformly distributed in the array, $\mathbf{p}_\gamma$ and $\mathbf{p}_\beta$ are also orthogonal to $\mathbf{p}_\alpha$; this can be made mathematically precise, but the intuition is simple: a roll or pitch action employs roughly the same number of CW and CCW modules, and thus the net yawing torque is zero. The result of having a large number of modules N in the array is that the $e_i \to 0$, which results in $\overline{\overline{\mathbf{Q}}} \to \mathbf{I}_3$ and $\mathbf{Q} \to \mathbf{P}\mathbf{D}$. One could then use the following simple decoupling strategy:

$$\begin{aligned} \mathbf{q}_z &= \frac{\mathbf{p}_z}{\|\mathbf{p}_z\|^2} & \mathbf{q}_\gamma &= \frac{\mathbf{p}_\gamma}{\|\mathbf{p}_\gamma\|^2} \\ \mathbf{q}_\beta &= \frac{\mathbf{p}_\beta}{\|\mathbf{p}_\beta\|^2} & \mathbf{q}_\alpha &= \frac{\mathbf{p}_\alpha}{\|\mathbf{p}_\alpha\|^2} \end{aligned}$$

It can be shown that the elements of $\mathbf{Q}$ above are not a function of N. Thus the decoupling strategy is also independent of N.

This decoupling strategy has the desirable property of minimizing the inter-module shear stresses in the array resulting from pitch and roll errors. This is readily seen by substituting $\mathbf{Q}$ into the control strategy, Eq. 13, and analyzing the resulting expression. It is clear that the control input a_i increases linearly the further away a module is from the center of mass. As a result, the tangential forces acting along the sides of a module are minimized. This is an important feature because too much shear stress would cause the module(s) to break away from the main array.

Note that this control strategy only works if both $\mathbf{P}$ and $(\hat{I}_x, \hat{I}_y, \hat{I}_z)$ are known. Both of these can be computed if the position and the direction of propeller rotation for each module is known; this assumes that all modules are identically the same, and that the mass and mass moments of inertia are given. It follows that position and the direction of propeller rotation is the only information that needs to be communicated across the array before taking flight.

Now that the control strategy has been decoupled, one can consider each degree of freedom separately. For example, the following functions can be chosen:

$$f_z(z, \dot{z}) = -2\omega_z\zeta_z\dot{z} - \omega_z^2(z - z_d) \tag{14}$$

$$f_\gamma(\gamma, \dot{\gamma}) = -\hat{I}_x(2\omega_\gamma\zeta_\gamma\dot{\gamma} + \omega_\gamma^2\gamma) \tag{15}$$

$$f_\beta(\beta, \dot{\beta}) = -\hat{I}_y(2\omega_\beta\zeta_\beta\dot{\beta} + \omega_\beta^2\beta) \tag{16}$$

$$f_\alpha(\alpha, \dot{\alpha}) = -\hat{I}_z(2\omega_\alpha\zeta_\alpha\dot{\alpha} + \omega_\alpha^2\alpha) \tag{17}$$

where each degree of freedom is a second-order system with $(\omega_z, \omega_\gamma, \omega_\beta, \omega_\alpha)$ representing the natural frequencies of the system and $(\zeta_z, \zeta_\gamma, \zeta_\beta, \zeta_\alpha)$ representing the damping ratios. The variable z_d represents the desired hovering altitude. The natural frequencies and damping ratios are tuning parameters that depend on the DFA's mass moments of inertia, which is affected by the size and configuration of the array, see Eq.

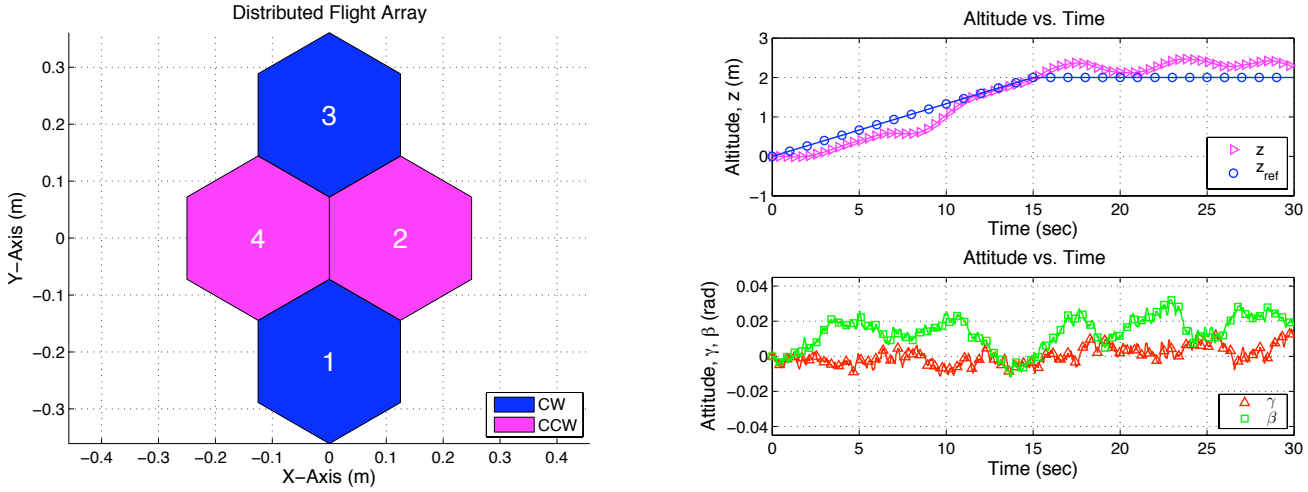

(a) (b)

Fig. 6. Simulation results for a 4-module configuration, where $(\omega_z, \omega_\gamma, \omega_\beta, \omega_\alpha) = (1.2, 13, 13, 1)$ and $(\zeta_z, \zeta_\gamma, \zeta_\beta, \zeta_\alpha) = (1, 1, 1, 1)$.

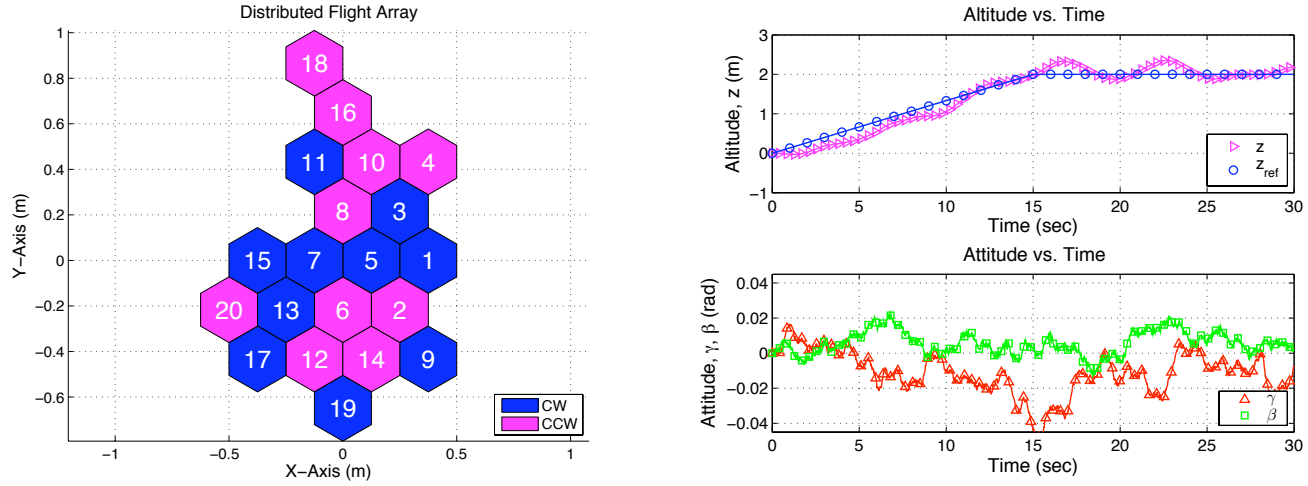

(a) (b)

Fig. 7. Simulation results for a 20-module configuration, where $(\omega_z, \omega_\gamma, \omega_\beta, \omega_\alpha) = (0.67, 5.81, 5.81, 0.45)$ and $(\zeta_z, \zeta_\gamma, \zeta_\beta, \zeta_\alpha) = (1, 1, 1, 1)$.

11. Note that the effect of array size is more pronounced in the yaw degree of freedom than in roll and/or pitch by a factor of $\sqrt{N}$.

This control strategy uses normalized thrust as the control input, which is not the case as described in Section III-B. Thrust dynamics and saturation of the control inputs should be considered. Time-scale separation is needed between the desired dynamics of the system and the rotor dynamics. A way to achieve this is to invert the transfer function G_f over a desired frequency range, enough to achieve time-scale separation.

This control strategy has been simulated in MATLAB for random array configurations consisting of 4 modules, up to 20 modules, see Fig. 6 – 7. Simulation experiments take into account sensor noise derived from physical experiments and the motor model described in Section III-B.

V. Experiments

The linear model presented in Section III and the results gathered from simulating the controller shown in Section IV were verified by testing the control strategy on the DFA in the array configuration shown in Fig. 2. Initial experiments established that the pressure sensor performed poorly and provided imprecise altitude measurements. Moreover, yaw control was intentionally left out to simplify the experiments. Consequently, experiments were made using only roll and pitch as feedback to the controller, see Eq. 15 – 16.

Before taking flight, the modules synchronized themselves via IrDA and calibrated their sensors by removing sensor offsets over a 5 second initialization sequence. Rate-gyro measurements were made at 200 Hz and the controller was operated at 60 Hz. The control input f_z was set to a very small value. A Vicon MX system [8] was used to measure both altitude and attitude of the DFA, see Fig. 8(b) – 8(c).

The DFA was shown to fly successfully with roll and pitch control. The experimental results look promising as they are comparable to the simulated system, thus verifying the utility of the linear model and simulator, see Fig. 8(a) – 8(b).

One interesting and unexpected result was observed due to yaw being left uncontrolled: the DFA ascended in a spiraling

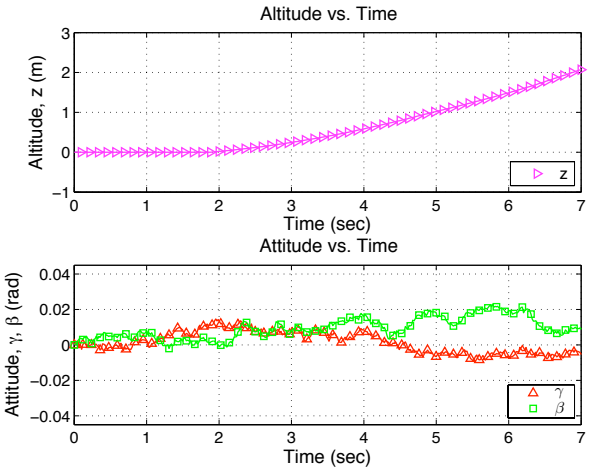

(a) Simulated results for a 4-module configuration without any feedback on altitude, where $(\omega_\gamma, \omega_\beta) = (13, 13)$ and $(\zeta_\gamma, \zeta_\beta) = (1, 1)$.

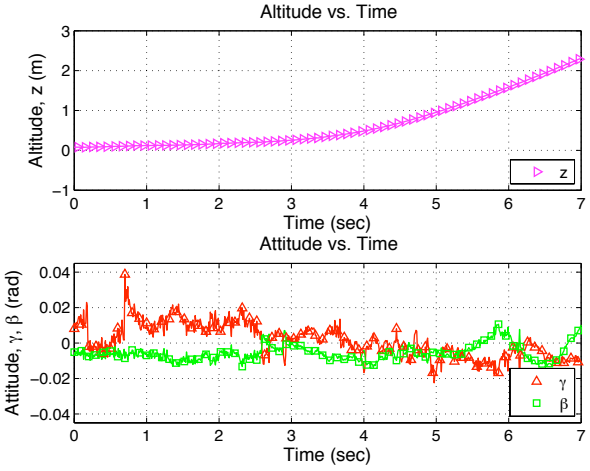

(b) The controller that was used in simulation, see Fig. 8(a), was also used in an experimental flight test; the measurements obtained from this test are shown here.

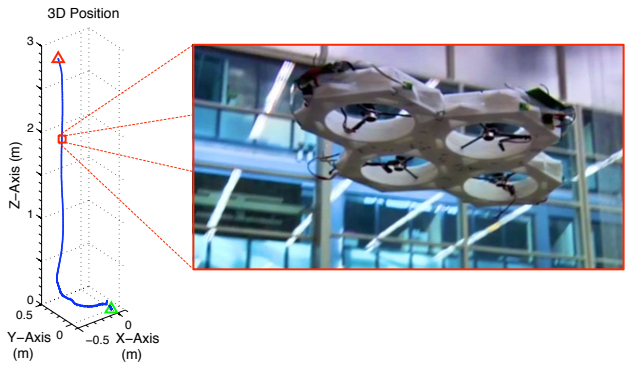

(c) A plot of the DFA's 3D position relative to its take-off origin, obtained from experimental results.

Fig. 8. Shown here are results gathered from a simulation and an experimental flight test without any feedback on altitude. Experimental measurements were made using a Vicon MX system.

motion, keeping its xy position of climb within the perimeter of the spiral. Assuming that γ and β are non-zero, and that the magnitude of α is increasing over time, this behavior is in fact expected due to the sine and cosine terms seen in Eq. 1 – 2. This then motivates the following constant yaw-rate control law:

$$f_\alpha(\dot{\alpha}) = -\hat{I}_z \omega_\alpha (\dot{\alpha} - \dot{\alpha}_d)$$

where $\dot{\alpha}_d$ is the desired yaw-rate.

VI. Conclusions and Future Work

This paper presented the Distributed Flight Array (DFA), a unique modular multi-rotor vehicle capable of autonomously self-assembling on the ground and taking flight. The DFA has been shown to fly both in simulation and in experiment by using a simple distributed strategy for hover control. The DFA is currently undergoing its second revision which will enable coordinated flight experiments on a larger scale. These results will be presented in future work.

VII. Acknowledgments

The authors would like to thank the team of technicians, researchers, and students of the 2008-2009 *!And Yet it Moves* class at ETH Zurich for their contribution to designing and constructing the initial DFA prototype. A special mention goes to Matthew Donovan and Frédéric Bourgault, from the same institution, for their contribution to the design of the modules.

References

[1] J. How, B. Bethke, A. Frank, D. Dale, and J. Vian, "Real-time indoor autonomous vehicle test environment," *Control Systems Magazine, IEEE*, vol. 28, no. 2, pp. 51–64, April 2008.

[2] G. Hoffmann, H. Huang, S. Waslander, and C. Tomlin, "Quadrotor helicopter flight dynamics and control: Theory and experiment," in *Proceedings of the AIAA Guidance, Navigation, and Control Conference*, Aug. 2007.

[3] S. Bouabdallah, M. Becker, and R. Siegwart, "Autonomous miniature flying robots: coming soon! - research, development, and results," *Robotics & Automation Magazine, IEEE*, vol. 14, no. 3, pp. 88–98, Sept. 2007.

[4] N. Guenard, T. Hamel, and V. Moreau, "Dynamic modeling and intuitive control strategy for an "x4-flyer"," in *Proceedings of the IEEE International Conference on Control and Automation*, vol. 1, June 2005, pp. 141–146.

[5] M. Yim, W.-M. Shen, B. Salemi, D. Rus, M. Moll, H. Lipson, E. Klavins, and G. Chirikjian, "Modular self-reconfigurable robot systems [grand challenges of robotics]," *Robotics & Automation Magazine, IEEE*, vol. 14, no. 1, pp. 43–52, March 2007.

[6] E. Klavins, "Programmable self-assembly," *Control Systems Magazine, IEEE*, vol. 27, no. 4, pp. 43–56, Aug. 2007.

[7] P. McKerrow, "Modelling the draganflyer four-rotor helicopter," in *Proceedings of the IEEE International Conference on Robotics and Automation*, vol. 4, May 2004, pp. 3596–3601.

[8] "Vicon mx homepage," Aug. 2009, [Accessed: Aug. 31, 2009]. [Online]. Available: http://www.vicon.com/products/viconmx.html